Simulated impacts of two types of ENSO events on tropical cyclone activity in the western North Pacific: large-scale atmospheric response

Chunxiang Li · Chunzai Wang

Abstract The present paper uses an atmospheric general circulation model to explore large-scale atmospheric response to various El Niño-Southern Oscillation events associated with tropical cyclone (TC) activity in the western North Pacific. The simulated response is basically consistent with and confirms the observed results. For eastern Pacific warm (EPW) event, anomalously wet ascent occurs over the tropical central/eastern Pacific and dry descent is over the western Pacific. This Walker circulation is associated with anomalous low-level convergence, reduced vertical wind shear (VWS), and enhanced genesis potential index (GPI) in the southeast sub-region. These are consistent with the observed increase of the TC formation in the southeast sub-region but decrease in the northwest sub-region during July–September (JAS) and the increase in the southwest and northwest sub-regions during October–December (OND). In addition, the strong westerly anomalies of the TC steering flow prevail in the East Asian coast, suppressing the TC northwestward or westward

tracks. For eastern Pacific cold (EPC) event, all of the simulated variables show almost a mirror image of EPW. For central Pacific warm event, the anomalous Walker circulation shifts westward because of the westward shift of the maximum SST anomaly forcing. The anomalous subsidence associated with the western branch of the Walker circulation during OND shifts northward to the South China Seas, resulting in a decrease of the TC genesis there. The TC steering flow patterns during JAS are favorable for TCs to make landfall over Japan and Korea. Compared with EPC, the descending motion in the central/eastern Pacific is much stronger for central Pacific cold (CPC) event, accompanied by more enhanced VWS and reduced GPI in the southeast sub-region. Therefore, CPC provides a more adverse environment to the TC formation there during JAS and OND, consistent with the observed decrease of TC formation there. Moreover, the easterly anomalies of the TC steering flow dominate the tropics during JAS, enhancing TC activity in the east coast of China. Additionally, the convection over the western Pacific moves to the South China Sea during OND, favoring the TC genesis there.

C. Li
Key Laboratory of Regional Climate-Environment Research for East Asia, Institute of Atmospheric Physics, Chinese Academy of Sciences, Beijing, China

C. Li
LASG/Institute of Atmospheric Physics, Chinese Academy of Sciences, Beijing, China

C. Wang (✉)
Physical Oceanography Division, NOAA Atlantic Oceanographic and Meteorological Laboratory, 4301 Rickenbacker Causeway, Miami, FL 33149, USA
e-mail: Chunzai.Wang@noaa.gov

1 Introduction

El Niño-Southern Oscillation (ENSO) is regarded as one of the most important climate phenomena affecting tropical cyclone (TC) activity (e.g., Chan 2000; Wang and Chan 2002; Wu et al. 2004; Camargo and Sobel 2005; Zhao et al. 2010). Recently, ENSO events have been separated into two types due to the different spatial distribution of the maximum sea surface temperature (SST) anomalies (Larkin and Harrison 2005; Ashok et al. 2007; Yu and Kao 2007; Kao and Yu 2009; Yu and Kim 2010). For eastern

Pacific ENSO events (also called canonical or conventional ENSO events), the maximum SST anomalies are generally located in the cold tongue region of the eastern Pacific. In contrast, central Pacific ENSO events (also called ENSO Modoki or Dateline ENSO) are characterized by the maximum SST anomalies in the central Pacific further west than canonical ENSO. The two types of ENSO events appear to induce distinct climatic and synoptic variability in various regions around the globe (e.g., Weng et al. 2007; Ashok and Yamagata 2009; Cai and Cowan 2009; Wang and Wang 2013). Wang et al. (2014) provide an ENSO overview including the two types of ENSO events and their different climate impacts and mechanisms.

Many studies have investigated the impacts of eastern and central Pacific ENSO events on TC activity (e.g., Kim et al. 2009; Lee et al. 2010; Chen and Tam 2010; Chen 2011; Kim et al. 2011; Larson et al. 2012; Zhang et al. 2012; Wang and Wang 2013). Wang et al. (2013) further explored the different impacts of eastern Pacific warm/cold (EPW/EPC) and central Pacific warm/cold (CPW/CPC) events on TC activity in the western North Pacific (WNP) during different seasons. Based on the analyses of observational data, they made several conclusions. First, during the early season (April to June, AMJ), EPW (EPC) is associated with a significant increase of the TC genesis number in the southeastern (southwestern) sub-region of the WNP. Meanwhile, EPW is associated with the TC steering flow patterns favoring TCs to take the recurving track and suppress the straight westward and northwestward tracks. Second, during the peak season (July–September, JAS), EPW corresponds to a significant enhancement (reduction) of the TC genesis in the southeastern (northwestern) sub-region, but CPW shows no significant change. EPC increases the TC genesis in the northwestern and northeastern sub-regions, but decreases the TC number in the southwestern portion. CPC suppresses the TC genesis in the southeastern sub-region (Fig. S1a). Moreover, EPW is associated with the TC steering flows which are not favorable for TCs to move northwestward or westward, whereas CPW favors the northwestward track and prevents the straight westward track (Fig. S2). Third, during the late season (October–December, OND), EPW reduces the TC genesis in the southwestern and northwestern sub-regions, while EPC (CPW) enhances the genesis in the northwestern (southeastern) sub-region. Over the South China Sea, CPW and CPC show a significant decrease and increase of the TC genesis, respectively (Fig. S1b). Furthermore, the TC steering flow patterns during OND are similar to those during JAS, except that EPC may increase the possibility of the northwestward track (Fig. S3).

Due to the limited ENSO events (particularly for CPW/CPC events) during the period of 1950–2009 and the

uncertainties of the observed data sets especially the TC data, it is necessary and important to use model experiments to confirm the observed results presented in Wang et al. (2013). The present paper is an extended work of the data analyses of Wang et al. (2013) by using an atmospheric general circulation model to study the response of large-scale environmental factors to two types of ENSO events associated with TC activity in the WNP. As the variability of the TC genesis and track during AMJ is relatively weak, this paper mainly focuses on two seasons of JAS and OND. Section 2 describes the data sets and numerical model as well as experiment designs used in this study. Section 3 demonstrates the model response of large-scale environmental factors that affect TC activity in the WNP. Section 4 shows the model response of the TC steering flow, and Sect. 5 presents the model response of the Walker circulation. Finally, a summary is given in Sect. 6.

2 Data sets and model experiment designs

Monthly SST from the Hadley Centre Global Sea Ice and Sea Surface Temperature (HadISST) for the years between 1950 and 2009 on a 1° latitude–longitude grid (Rayner et al. 2003) is used to force the atmospheric model. Atmospheric data set is the updated National Centers for Environment Prediction (NCEP)/National Center for Atmospheric Research (NCAR) reanalysis with a spatial resolution of 2.5°×2.5° (Kalnay et al. Kalnay et al. 1996), which is used to compare with model results. Based on the TC data from China Meteorological Administration (CMA), we also show some of the observed TC activity and the association of TC activity with the two types of ENSO events in Appendix 1 and Appendix 2.

The atmospheric general circulation model (AGCM) used in this study is the ECHAM5 developed by the Max Planck Institute for Meteorology (Roeckner et al. 2003). It is a global spectral model with a triangular spectral truncation of the spherical harmonics at zonal wavenumber 42 (T42), roughly equivalent to 2.8° latitude by 2.8° longitude. The model is vertically divided into 19 levels in a hybrid sigma-pressure layers from the surface to 10 hPa.

In our observational paper (Wang et al. 2013), the Nino3 (5°N–5°S, 150°W–90°W) and Nino4 (5°N–5°S, 160°E–150°W) SST anomalies as well as SST spatial distribution are used to describe EP and CP warm/cool events. EPW (EPC) events are associated with the maximum SST anomalies in the eastern Pacific and require that the 5-month running means of SST anomalies in the Nino3 region exceed 0.5°C (−0.5°C) for at least 6 months. CPW (CPC) events are defined if the 5-month running mean Nino4 SST anomalies are +0.5°C (−0.5°C) or higher

(lower) for six consecutive months or longer and the maximum SST anomalies are located in the central Pacific. Based on these criteria and the SST data from 1950 to 2009, 8 EPW years (1951, 1957, 1965, 1972, 1976, 1982, 1987, 1997), 8 EPC years (1955, 1964, 1967, 1971, 1984, 1985, 1988, 2007), 5 CPW years (1969, 1991, 1994, 2002, 2004) and 5 CPC years (1973, 1975, 1989, 2000, 2008) can be identified. The composites of SST anomalies for EPW, EPC, CPW and CPC events during the mature phase of ENSO are shown in Fig. 1.

To examine the response of various ENSO events, we conduct five sets of model experiments: CTRL, EPW, EPC, CPW, and CPC runs. In the CTRL run, the model is globally forced by the monthly climatological SST. In the

Fig. 1 Composites of SST anomalies (°C) during the mature phase of ENSO (November–January) for **a** EPW, **b** EPC, **c** CPW, and **d** CPC events
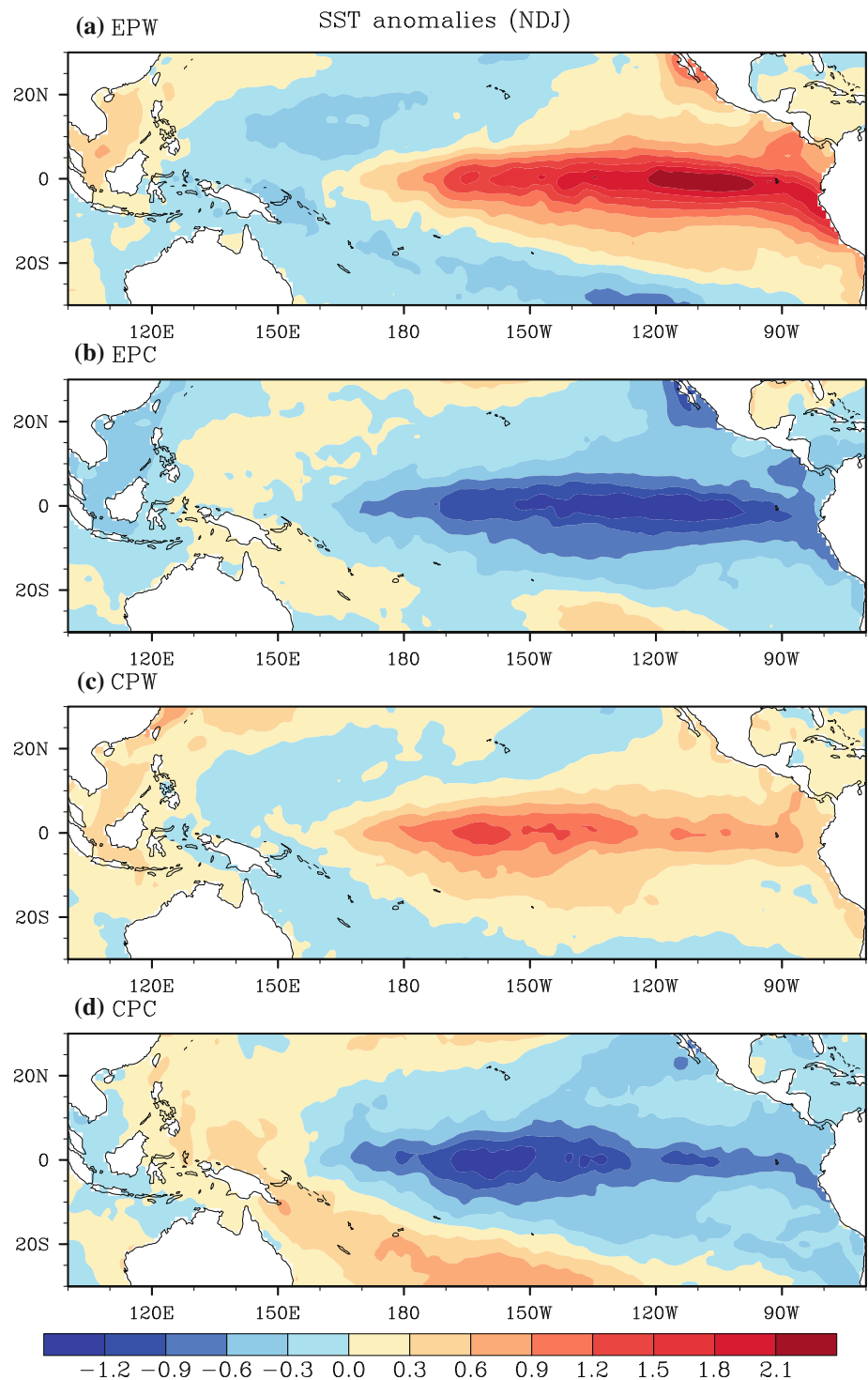
EPW/EPC (CPW/CPC) experiments, the composited 12-monthly SST anomalies for the EPW/EPC (CPW/CPC) events are added to the climatological SST in the tropical Pacific (from 30°S to 30°N between 105°E and the coast of Americas), while the climatology is applied in the rest of global ocean. For each set of simulations, the model is integrated for 20 years. The first 2 years of outputs are discarded to exclude any possible transient spinup effects. A time mean is then calculated by averaging the output of the remaining 18-year for each season. On the assumption that each year is statistically independent, this is equivalent to an ensemble mean with 18 members. To examine the effect of ENSO events, we calculate the differences between the individual model run of various ENSO events and the CTRL run.

3 Simulated response of large-scale environmental factors

TC activity is influenced by large-scale dynamical (e.g., low-level vorticity and vertical wind shear) and thermo-dynamical (e.g., atmospheric stability and mid-level moisture) factors (e.g., Gray 1979). In this section, we first examine the model response of dynamical factors to various ENSO events: the relative vorticity and wind at 850 hPa, and the vertical wind shear. We then focus on the simulated genesis potential index—the combination of all large-scale environmental factors. Since both atmospheric circulation in the WNP and ENSO vary seasonally and most of TCs occur in the summer and fall, we focus on the model response during July–September (JAS) and October–December (OND).
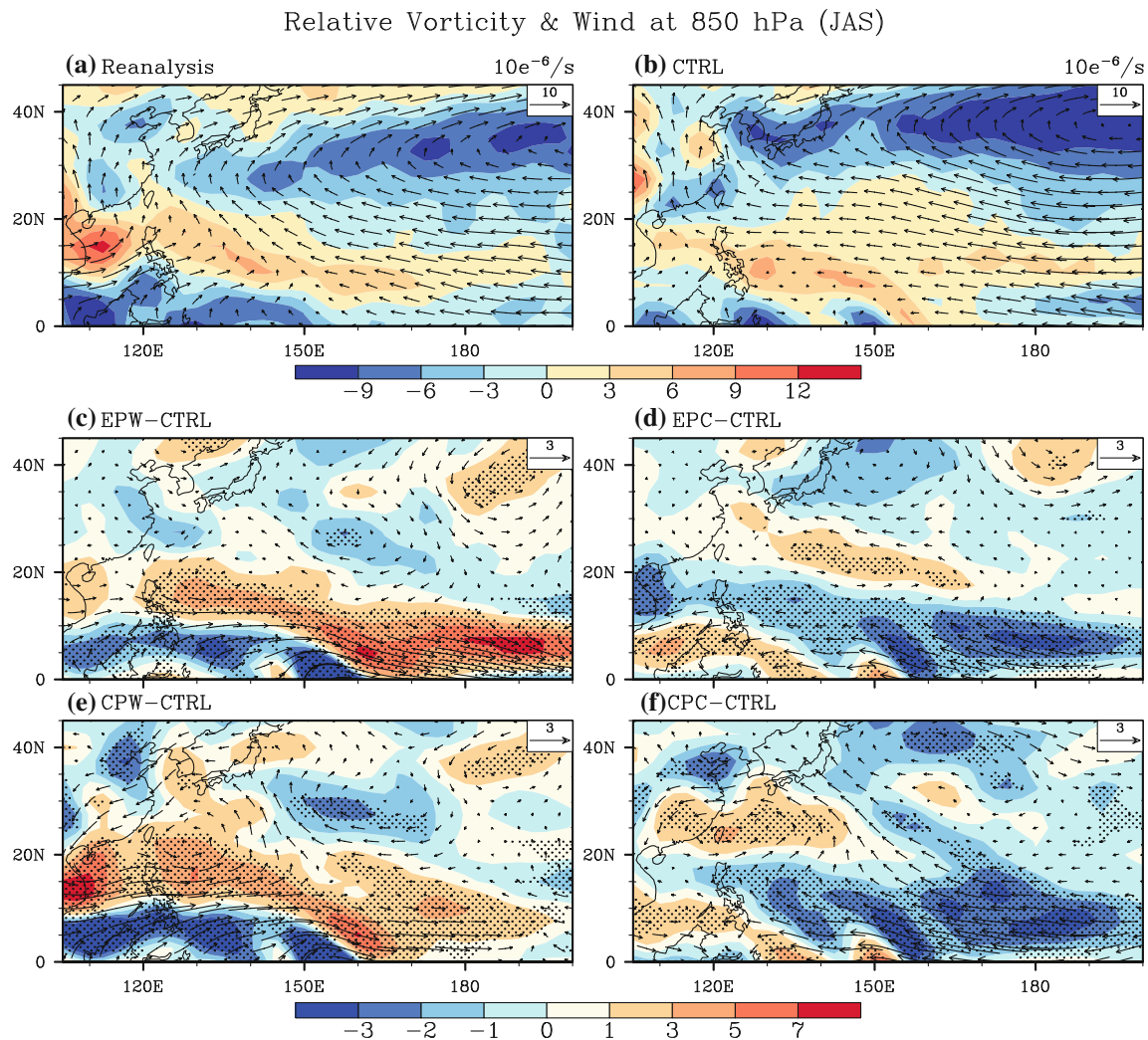
3.1 Relative vorticity and wind at 850-hPa

The western North Pacific subtropical high (WNPSH) is an important phenomenon for influencing atmospheric circulation in the WNP. The mean anticyclonic circulation associated with the WNPSH is clearly seen in JAS and OND, with the easterly trade and westerly winds in its southern and northern sides, respectively (Figs. 2a, 3a). The WNPSH shifts equatorward and westward in OND. Over the South China Sea (SCS), the southwesterly wind during JAS switches into the northeasterly winter monsoon during OND. Associated with these mean wind distributions are the positive mean relative vorticity in the tropical region and the negative mean relative vorticity in the subtropical region. The CTRL model run does a reasonably good job in simulating the climatological atmospheric circulation in the WNP (Figs. 2b, 3b). However, the simulated WNPSH is slightly stronger than that of the NCEP–NCAR reanalysis. The simulated distributions of positive

and negative relative vorticity are basically similar to the reanalysis. As shown in Table 1, the pattern correlations of the relative vorticity between the CTRL run and the NCEP–NCAR reanalysis are 0.53 and 0.84 during JAS and OND, respectively.

The difference between the EPW and CTRL runs shows strong westerly wind anomalies south of 14°N associated with the returned branch of the Walker circulation induced by El Niño event (Figs. 2c, 3c). The maximum westerly anomalies are located around 10°N in the west of the WNP and shift equatorward toward the east. The anomalous anticyclone in the subtropical WNP (Weisberg and Wang 1997; Wang et al. 1999) is also simulated in the EPW run, especially during OND. These wind patterns produce a vorticity distribution that shows a band of positive relative vorticity anomalies spanning from the southeastern (SE) sub-region to the south coast of China and being flanked by the negative anomalies to its south and north (Figs. 2c, 3c). Note that the tropical WNP is partitioned into four sub-regions (140°E and 17°N serve as the borders between the east and west and between the south and north, respectively): the southwestern (SW), northwestern (NW), northeastern (NE) and southeastern (SE) portions (e.g., Wang and Chan 2002; Wang et al. 2013). The maximum positive vorticity anomalies are located in the SE sub-region, consistent with that EPW events are favorable for the formation of TCs in the SE sub-region (Fig. S1a). The simulated relative vorticity anomalies in the NW sub-region do not show a negative value, suggesting that the observed decrease of the TC formation there is not due to the vorticity change. The simulated response for the EPC run is similar to that of the EPW run, but with the anomaly sign reversed (Figs. 2d, 3d).

For CPW events, the SE-NW positive relative vorticity anomalies and the westerly wind anomalies in the equatorial central Pacific move westward in comparison with EPW events (Figs. 2e, 3e), consistent with the distributions of SST anomaly forcing (Fig. 1). Another feature is that the positive vorticity anomalies in the SE sub-region during OND is larger than those during JAS (Figs. 2e vs. 3e), reflecting that OND is closer to the mature phase of El Niño event. Additionally, the model CPW run shows that an anomalous cyclone is located northeast of the Philippine Sea, especially during JAS. The anomalous cyclone reflects Gill's (1980) response to the warm SST anomalies in the equatorial central Pacific. This is consistent with the result of Wang and Wang (2013) who observed an anomalous cyclone in the WNP for some of CPW events. In contrast to EPC, much stronger negative vorticity and easterly wind anomalies can be found in the SE sub-region during two seasons of CPC years, providing a more adverse environment to TC activity there. Due to the positive SST anomalies in the western Pacific (shown in Fig. 1d), an

Relative Vorticity & Wind at 850 hPa (JAS)

Fig. 2 The distribution of 850-hPa relative vorticity (10^{-6}/s) and wind (m/s) during JAS in the WNP. Shown are the climatological means from **a** the NCEP–NCAR reanalysis and **b** the CTRL ensemble run. The differences between the EPW, EPC, CPW, and CPC runs and the CTRL run are shown in **c, d, e**, and **f**, respectively. The *stippling* indicates the statistical significance of relative vorticity at the 95 % level

anomalous cyclone is found near Taiwan. Moreover, during OND, the northeasterly wind related to the cyclone merges with the equatorial westerlies, inducing the positive relative vorticity anomalies over the SCS, which is conducive to the enhanced TC activity in the SCS as observed in Fig. S1b.

3.2 Vertical wind shear

As in other studies, the vertical wind shear (VWS) is calculated as the magnitude of the vector difference between winds at 200 and 850 hPa. The climatological VWS patterns during two seasons of JAS and OND are different (Figs. 4a, 5a). During JAS, the VWS in the WNP shows a V pattern, with a low wind shear in the southern, northern and western sides of the WNPSH. However, the VWS

during OND features a low wind shear in the tropical WNP and a high value in the subtropical WNP. Overall, the simulated VWS in the CTRL model run compares well with the observation: the pattern correlations are 0.59 and 0.97 during JAS and OND, respectively (Table 1).

The model simulated VWS patterns for EPW and EPC events are similar to those from the NCEP–NCAR reanalysis as shown in Wang et al. (2013). For EPW events, the negative VWS anomalies reside in the SE subregion of the WNP, while the positive VWS anomalies are located just north of the equator in the western Pacific (Figs. 4c, 5c). This is because the Walker circulation is weakened during an El Niño event (see Sect. 5 for the details), which manifests itself as a suppressed convection in the western Pacific and an enhanced convection in the central/eastern Pacific. The negative VWS anomalies in the

Relative Vorticity & Wind at 850 hPa (OND)
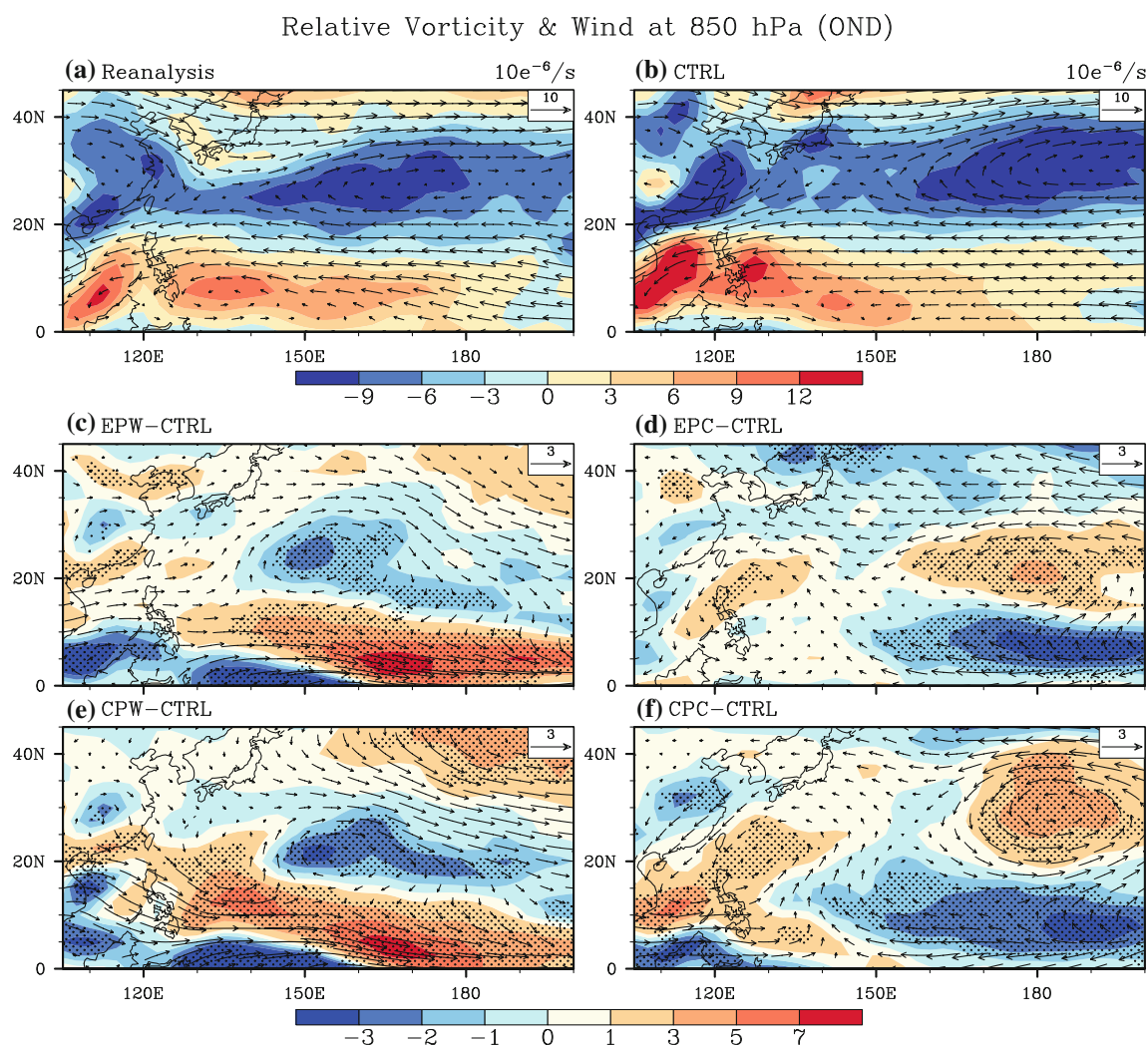
Fig. 3 The distribution of 850-hPa relative vorticity (10^{-6}/s) and wind (m/s) during OND in the WNP. Shown are the climatological means from **a** the NCEP–NCAR reanalysis and **b** the CTRL ensemble run. 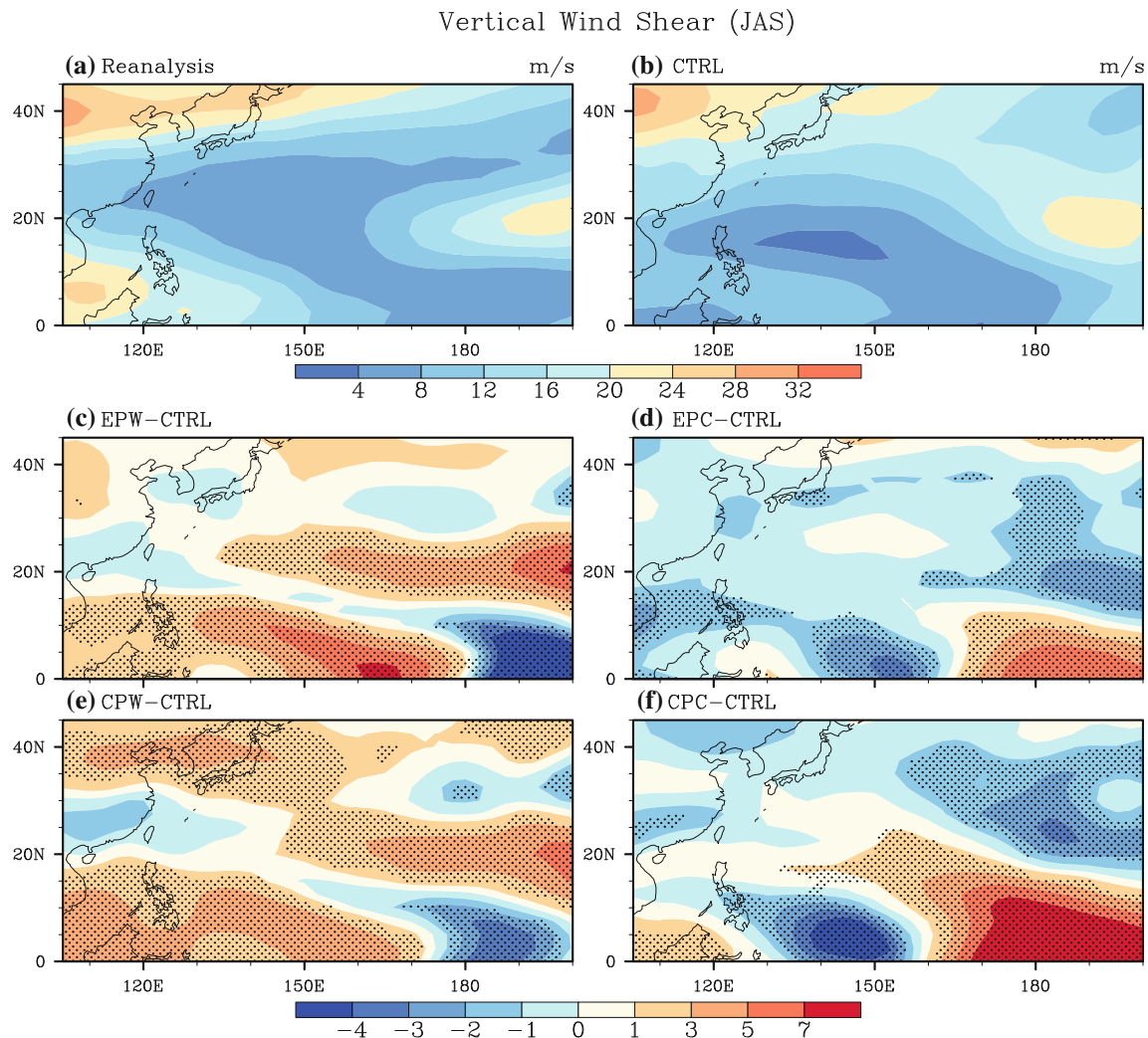The differences between the EPW, EPC, CPW, and CPC runs and the CTRL run are shown in **c**, **d**, **e**, and **f**, respectively. The *stippling* indicates the statistical significance of relative vorticity at the 95 % level

Table 1 The pattern correlation coefficients of the 850-hPa relative vorticity (VOR), vertical wind shear (VWS), genesis potential index (GPI), U and V component of the TC steering flow between the CTRL run and the NCEP–NCAR reanalysis during July–September (JAS) and October–December (OND)

Variable	VOR	VWS	GPI	U of steering flow	V of steering flow
Season					
JAS	0.53	0.59	0.92	0.93	0.41
OND	0.84	0.97	0.96	0.98	0.82

The coefficients measure the simultaneous spatial correlation between the observed and corresponding simulated fields with the sample size that is determined by the total number of grids in the region of 105°E–160°W, 0–45°N

SE sub-region during OND shifts westward compared to those during JAS, due to that the warm SST anomalies of an El Niño event during OND are larger and further westward than during JAS. This VWS distribution is consistent with that an EPW event is observed to be favorable for the formation and development of TCs in the SE sub-region (Fig. S1a). The positive VWS anomalies prevail over the most northern areas of the WNP, creating an unfavorable environment for the TC development, also consistent with the decrease of the TC genesis in the NW sub-region during two seasons (Fig. S1). Not surprisingly, the simulated response of the VWS for the EPC run is almost opposite to that of the EPW run (Figs. 4d, 5d), as did in the NCEP–NCAR reanalysis (Wang et al. 2013).
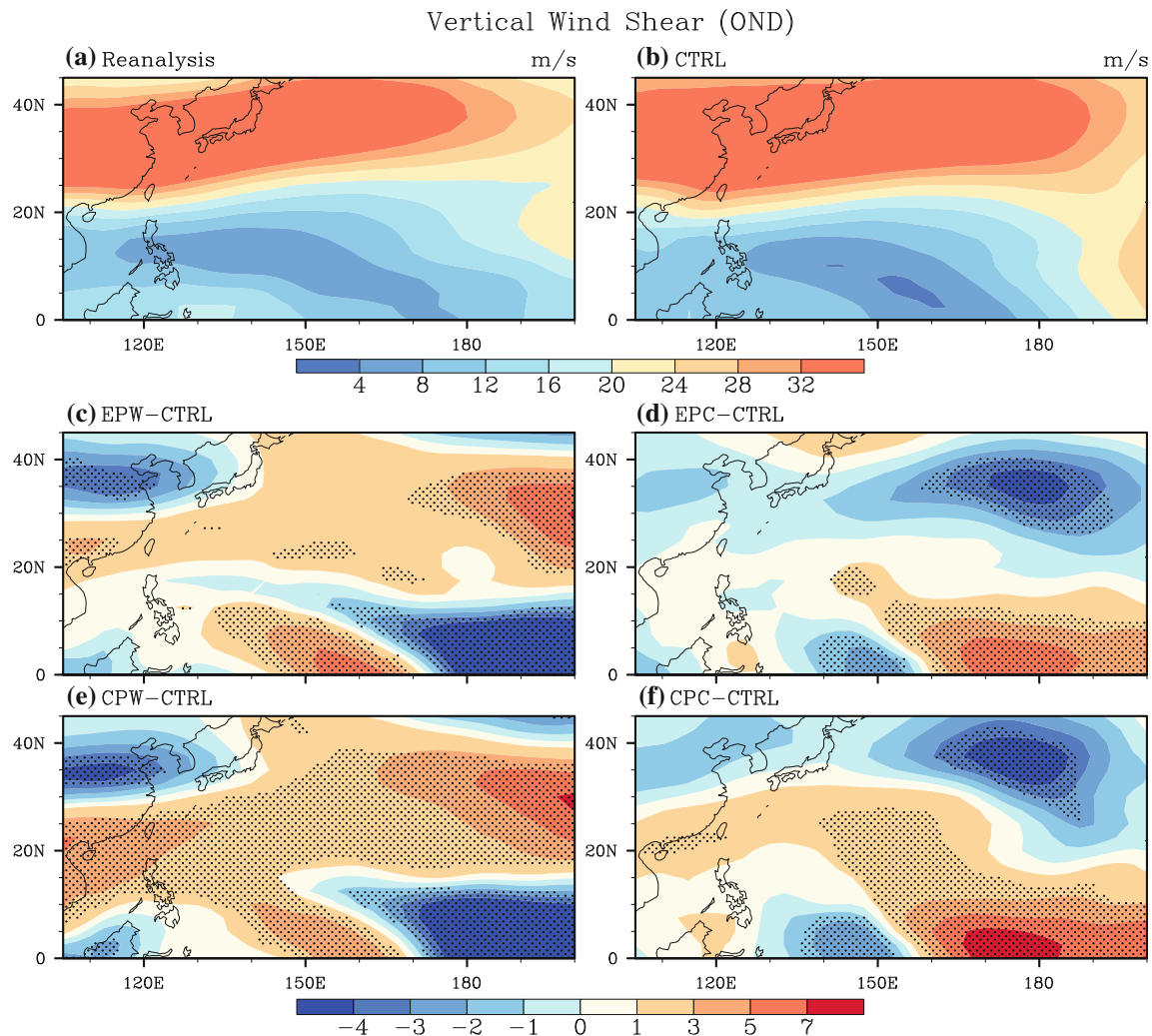
Vertical Wind Shear (JAS)

Fig. 4 The distribution of VWS (m/s) during JAS in the WNP. Shown are the climatological means from **a** the NCEP–NCAR reanalysis and **b** the CTRL ensemble run. The differences between the EPW, EPC, CPW, and CPC runs and the CTRL run are shown in **c**, **d**, **e**, and **f**, respectively. The *stippling* indicates the statistical significance at the 95 % level

In comparison with the EPW run, the model VWS response of the CPW run shows a similar pattern except the westward shift of the VWS anomalies. This is consistent with the westward shift of the maximum positive SST anomalies for CPW events. The VWS response is also consistent with and supports the observed result which shows the decrease of the TC genesis in the SCS and increase in the SE sub-region during OND (Fig. S1b). The model VWS pattern in the CPC run is almost a mirror image of the CPW run. Another feature is that the magnitude of positive VWS anomalies in the SE sub-region for the CPC run is much larger than that of the EPC run (see Sect. 5 for the details associated with the more intense Walker circulation). Therefore, CPC-induced VWS is more unfavorable for the TC genesis and development in the SE sub-region.

3.3 Genesis potential index

TC activity is influenced by the combination of all large-scale environmental factors. Emanuel and Nolan (2004) developed an empirical index, the Genesis Potential Index (GPI), to combine the influence of all variables on the TC genesis. Climatologically, the great values of the GPI are concentrated in the tropics of the WNP (Figs. 6a, 7a). During JAS, the value of GPI is much greater and the large value area is more extensive than that during OND, consistent with that JAS is the peak season for TCs in the WNP. Meanwhile, there is a seasonal march of GPI with a northward (southward) migration during JAS (OND), reflecting that most TCs form in the north and move northwestward during JAS, but they tend to form in the south and take a straight westward track during OND.

Vertical Wind Shear (OND)

Fig. 5 The distribution of VWS (m/s) during OND in the WNP. Shown are the climatological means from **a** the NCEP–NCAR reanalysis and **b** the CTRL ensemble run. The differences between the EPW, EPC, CPW, and CPC runs and the CTRL run are shown in **c**, **d**, **e**, and **f**, respectively. The *stippling* indicates the statistical significance at the 95 % level

Although the model simulated GPI value is much higher (Figs. 6b, 7b), ECHAM5 captures the TC GPI regions and reproduces the observed spatial characteristics in comparison with the NCEP–NCAR reanalysis: The pattern correlations are 0.92 and 0.96 during JAS and OND, respectively. The model overvalued GPI may be due to the inflated relative humidity in the model simulation, as shown in Camargo et al. (2007).

For the EPW run, the GPI anomalies are positive in the SE sub-region of the WNP, whereas the rest regions mostly display the negative GPI anomalies during JAS and OND (Figs. 6c, 7c). The model simulated GPI anomaly patterns are consistent with those calculated from the NCEP–NCAR reanalysis (Wang et al. 2013). For the EPC run, the GPI anomalies in the SE and NW sub-regions are reversed to be negative and positive, respectively. These model GPI anomalies are consistent with the observed TC genesis that

for an EPW event, the number of TCs increases in the SE sub-region and decreases in the NW sub-region (Fig. S1). The opposite is true for an EPC event.

For the CPW run, the model simulated GPI anomalies are also similar to those from the NCEP–NCAR reanalysis in Wang et al. (2013), except the over-simulated negative GPI anomalies in the subtropical WNP. During OND, Fig. 7e shows the strong negative GPI anomalies in the SW sub-region and the SCS, consistent with the observed result of a decrease of the TC genesis in the SCS during OND of CPW years (Fig. S1b). The model simulated GPI anomalies in the CPC run are much closer to the NCEP–NCAR reanalysis. Both the reanalysis and simulation during JAS for CPC show a zonal dipole structure of the GPI anomalies with negative values in the east and positive values in the west (a southward contraction during OND). This suggests that during JAS of CPC years, atmospheric and

Genesis Potential Index (JAS)
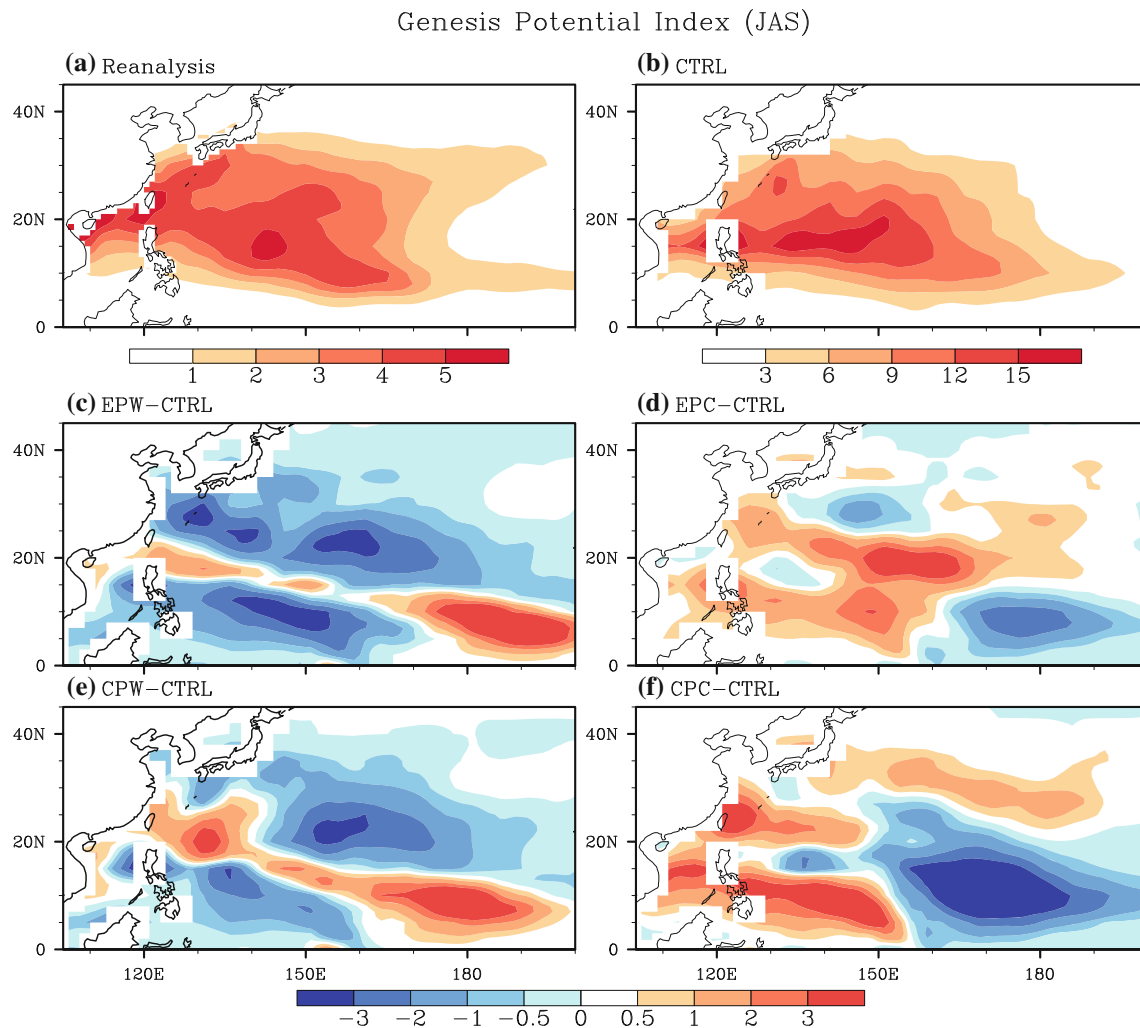
Fig. 6 The distribution of GPI during JAS in the WNP. Shown are the climatological means from **a** the NCEP–NCAR reanalysis and **b** the CTRL ensemble run. The differences between the EPW, EPC, CPW, and CPC runs and the CTRL run are shown in **c**, **d**, **e**, and **f**, respectively

oceanic conditions are unfavorable for TCs to form in the SE sub-region, but TCs are promoted in the SCS, which are consistent with the observations (Fig. S1).

4 Simulated response of the TC steering flow

The movement of TCs or the TC track is mainly steered by the surrounding environmental flow in the troposphere and modified by the beta-effect. An integrated flow through a layer of the atmosphere from 850 to 300 hPa is usually defined as the TC steering flow (e.g., Dong and Neumann 1986). During JAS and OND, the TC steering flows in the WNP manifest the WNPSH (Figs. 8a, 9a). The easterly, southeasterly and westerly TC steering flows are located in the southern, western and northern sides of the WNPSH, respectively. The ECHAM5 model is generally capable of capturing the basic features of the TC steering flow

although the centers of these steering flows are located slightly northeastward in the CTRL run (Figs. 8b, 9b). The respective pattern correlations of the U and V components of the TC steering flow are 0.93 and 0.41 (0.98 and 0.82) during JAS (OND).

The differences of the TC steering flows between the various ENSO event runs and CTRL run are basically consistent with the composites of the TC steering flow anomalies from the NCEP–NCAR reanalysis (Figs. S2, S3). During JAS, the TC steering flow for EPW is associated with the westerly anomalies in the tropics and an anomalous cyclone in East Asian (Fig. 8c). This TC steering flow pattern is unfavorable for TCs to take a straight westward track and suppresses the possibility for TCs to make landfall in the southeast coast of China (Wang and Chan 2002; Zhang et al. 2012; also shown in Fig. S2a). For EPC, the simulated TC steering flows show the easterly anomalies in the tropics and the southeasterly anomalies in
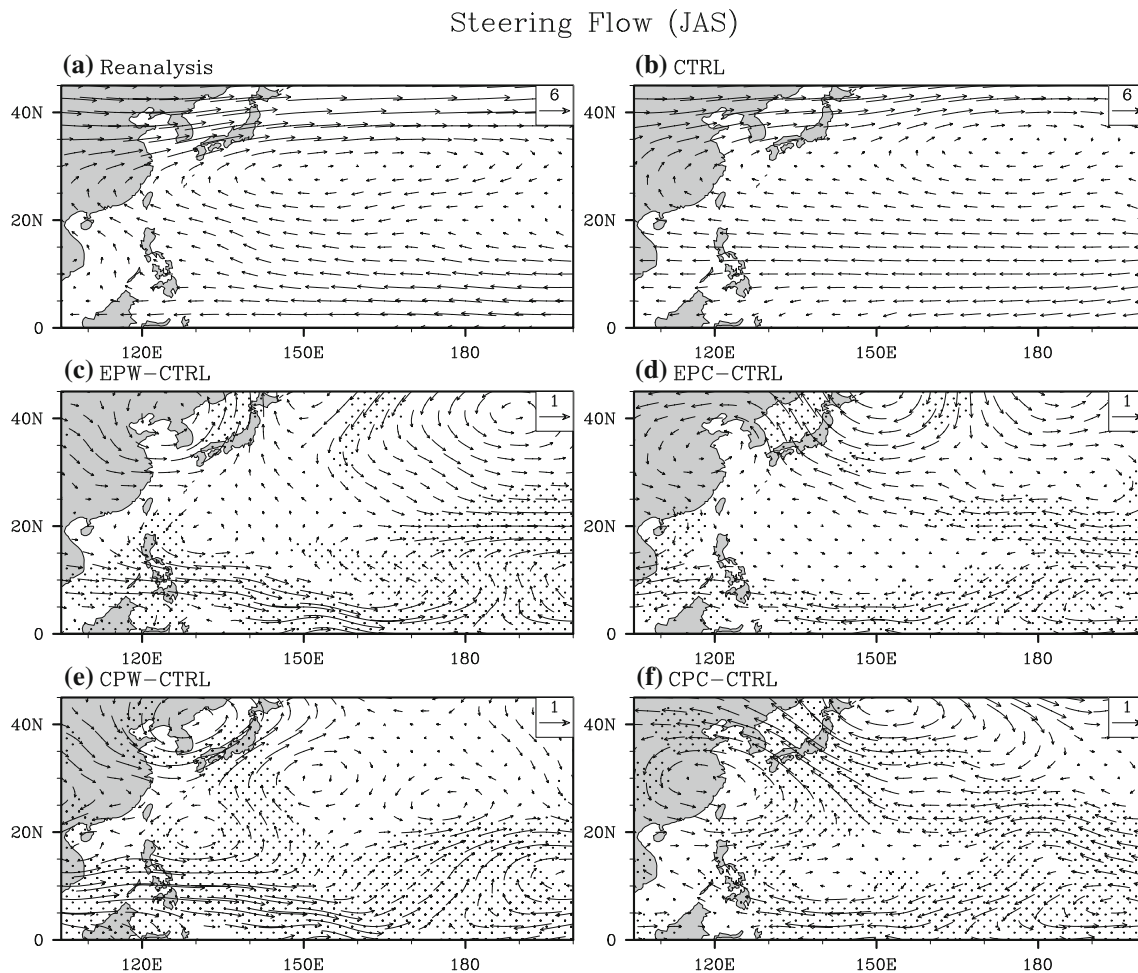
Genesis Potential Index (OND)
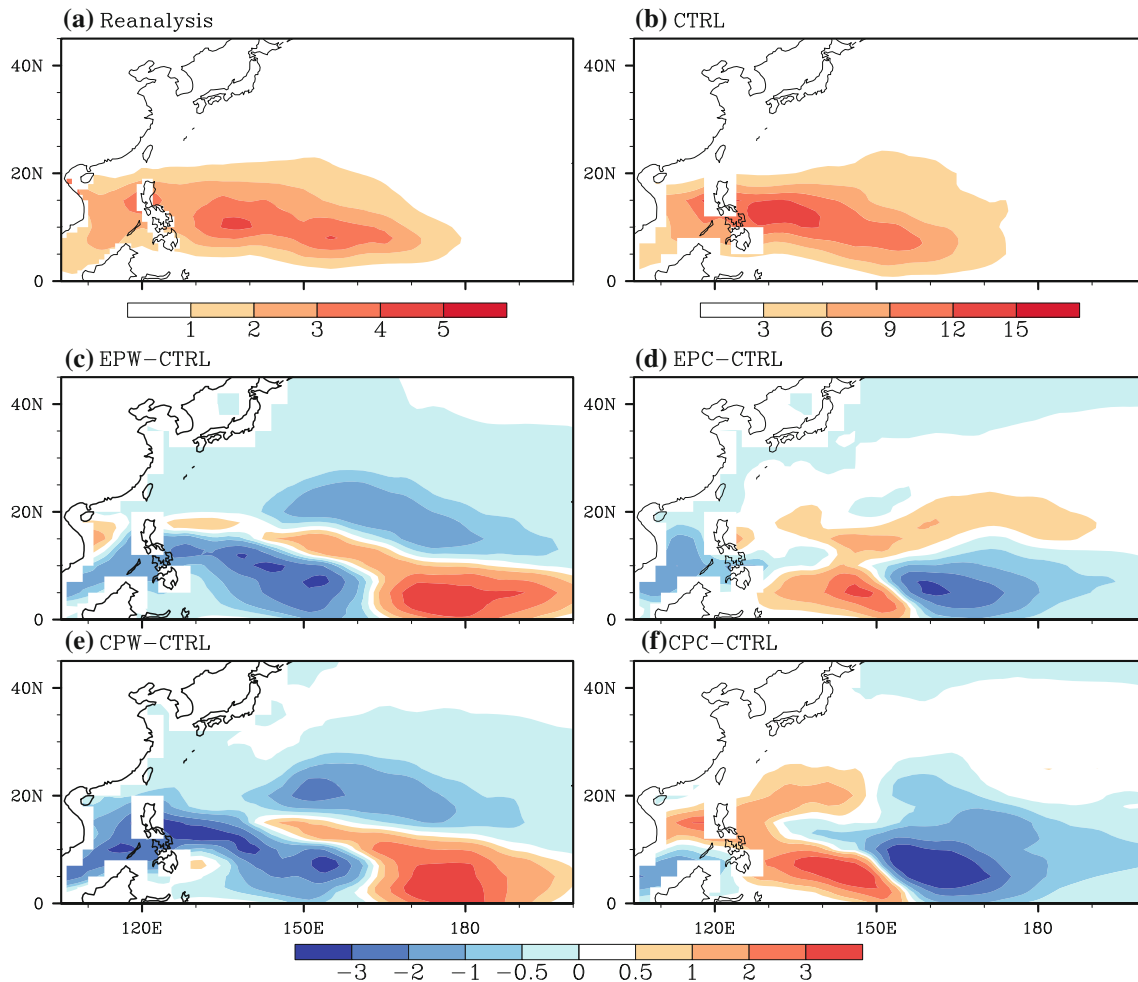
Fig. 7 The distribution of GPI during OND in the WNP. Shown are the climatological means from **a** the NCEP–NCAR reanalysis and **b** the CTRL ensemble run. The differences between the EPW, EPC, CPW, and CPC runs and the CTRL run are shown in **c**, **d**, **e**, and **f**, respectively

Japan and the subtropical WNP. The TC steering flow for CPW shows the westerly anomalies over the tropics south of 15°N, an anomalous cyclone in the northeast of Philippines and an anomalous anticyclone in the southeast of Japan (Fig. 8e), which is located slightly southeastward in comparison with the observed results in Fig. S2c. Therefore, the TC steering flows tend to lead to the northwestward track and suppress the westward track, consistent with the distributions of the observed TC track density (Kim et al. 2011; Fig. S2c). For CPC, there are a well-organized large-scale anomalous cyclonic circulation over eastern China and the easterly anomalies in the tropics (Fig. 8f). It is clear that the TC steering flow anomalies for CPC are favorable for TCs to move westward and northwestward, but hostile to the recurvature track.

During OND, the observed TC steering flow anomalies for EPW show an anomalous anticyclone over the Philippines (Fig. S3a). This pattern shifts to the central portion of

the WNP with southwesterly anomalies over the seaboard of East Asia in the model simulation (Fig. 9c). It may be as a result of the eastward contraction of the WNPSH in simulation compared to the observation (not shown). For EPC, due to the local warm SST anomalies in the WNP (Fig. 1b), an anomalous cyclone is found over the east of the WNP, associated with strong easterly anomalies of the TC steering flow in the subtropical ocean. For CPW, the westerly anomalies of the TC steering flow cover the tropical WNP (Fig. 9e), consistent with Zhang et al. (2012) who observed fewer landfalls over Indo-China and Malay Peninsula and Philippines during CPW years. For CPC, although the simulated TC steering flow anomalies are mostly westerly or southwesterly in the tropical WNP, there is an observed enhancement of TC track density in the east coast of China (Fig. S3d) associated with the increase of TC genesis in the SCS and NW sub-region (Fig. S1b).

Steering Flow (JAS)

Fig. 8 The distribution of the TC steering flow (m/s) during JAS in the WNP. Shown are the climatological means from **a** the NCEP–NCAR reanalysis and **b** the CTRL ensemble run. The differences between the EPW, EPC, CPW, and CPC runs and the CTRL run are shown in **c**, **d**, **e**, and **f**, respectively. The *stippling* indicates the statistical significance at the 95 % level

5 Simulated response of the Walker circulation

The Walker circulation is an important feature of ENSO, which is associated with the variations of atmospheric convection in the tropical Pacific and is thus related to TC activity in the WNP. The Walker circulation and the vertical profile of specific humidity during two seasons of JAS and OND are shown in Figs. 10 and 11, respectively. Climatologically, the tropical Pacific is dominated by a well-organized Walker circulation with ascending motion in the equatorial western Pacific and descending motion in the equatorial eastern Pacific (Julian and Chervin 1978). Connected the upward and downward branches are the upper level westerly wind and returned low-level easterly wind. ECHAM5 simulates these features reasonably well, as shown in Figs. 10b and 11b.

For the EPW run, the anomalous Walker circulation in the tropical Pacific shows anomalously wet updraft over the central Pacific and dry downdraft over the western

Pacific. Accompanied with these are the westerly wind anomalies at the low level extending from 120°E to the central Pacific during two seasons (Figs. 10c, 11c). These indicate an anomalous low-level cyclonic (anticyclonic) vorticity and enhanced (suppressed) convection over the SE (SW) sub-region of the WNP, consistent with the significantly increased (decreased) TC formation in the SE (SW) sub-region during JAS (OND). The simulated Walker circulation change is also consistent with the VWS variations (Figs. 4, 5), which shows that the anomalous dry downward (wet upward) motion in the western (central) Pacific is associated with an increased (decreased) VWS and thus a suppressed (enhanced) convection.

For CPW, along with the westward shift of SST anomaly forcing, the Walker circulation shifts westward during two seasons (Figs. 10e, 11e). Most of the central-eastern tropical Pacific regions is dominated by a wet ascending branch, spanning over 150°E–140°W, flanked by the dry descending movements west of 150°E and east of 120°W. Compared

Steering Flow (OND)
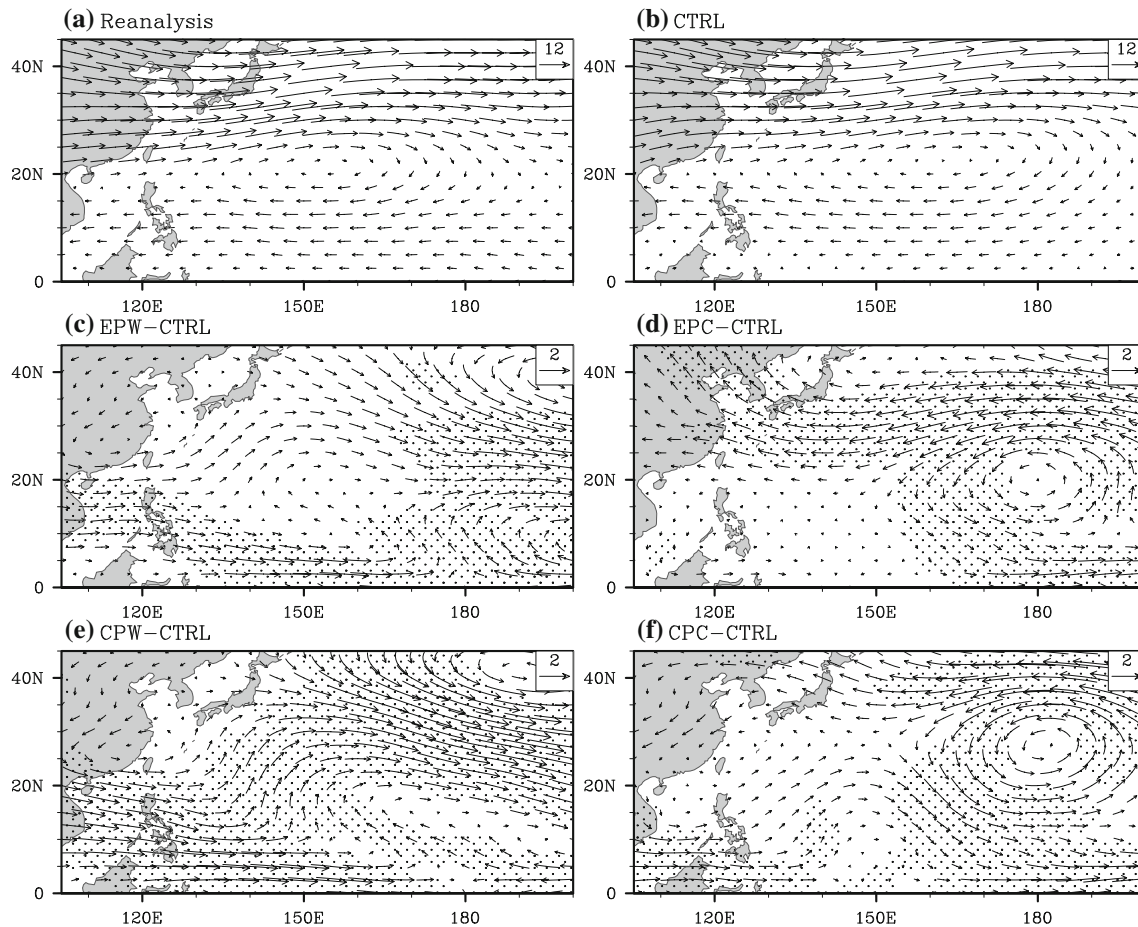
Fig. 9 The distribution of the TC steering flow (m/s) during OND in the WNP. Shown are the climatological means from **a** the NCEP–NCAR reanalysis and **b** the CTRL ensemble run. The differences between the EPW, EPC, CPW, and CPC runs and the CTRL run are shown in **c**, **d**, **e**, and **f**, respectively. The *stippling* indicates the statistical significance at the 95 % level

with the case during JAS, the rising branch during OND shifts eastward and is reinforced with the development of the maximum warm SST anomalies in the central equatorial Pacific. In other words, the arising motion near the dateline is stronger during OND, corresponding to the remarkable increase of the TC formation in the SE sub-region in the observation (Fig. S1b). In addition, the subsidence during OND shifts westward, which is related to the feature that the anomalous descending motion moves westward and extends to the north of the SCS (Weng et al. 2009). This explains why there is an observational suppression of the TC formation in the SCS during OND of CPW years.

Comparing the two warm events, the descent over Indonesia in EPW (CPW) is slightly stronger (weaker) and tends to appear further eastward (westward). Consequently, it is more likely that EPW and CPW inhibits the TC formation in the SW sub-region of the WNP and the SCS, respectively (Fig. S1). Furthermore, during the two seasons, the ascent over the central-eastern Pacific is located

further westward in CPW than the counterpart of EPW, which is more evident during JAS than that during OND (Figs. 10c, e vs. 11c, e). This is consistent with the evolution of the SST anomalies in the two types of warm events presented in previous studies (e.g., Kao and Yu 2009; Kug et al. 2009; Wang et al. 2014). That is, the positive SST anomalies emerge from the coast of South America and propagate westward to the central Pacific with the development of EPW, while the SST anomalies first appear around the dateline and develop slowly without any significant movement in CPW events. In addition, the Walker circulation variations of ENSO warm events are associated with a tripole pattern of the humidity anomalies: Negative–Positive–Negative humidity anomalies.

For EPC, the anomalous Walker circulation during JAS displays a pattern with rising in the west of 150°E and sinking in the east (Figs. 10d, 11d), reflecting an intensification of the Walker circulation. Associated with the intensified Walker circulation, the tropical Pacific is
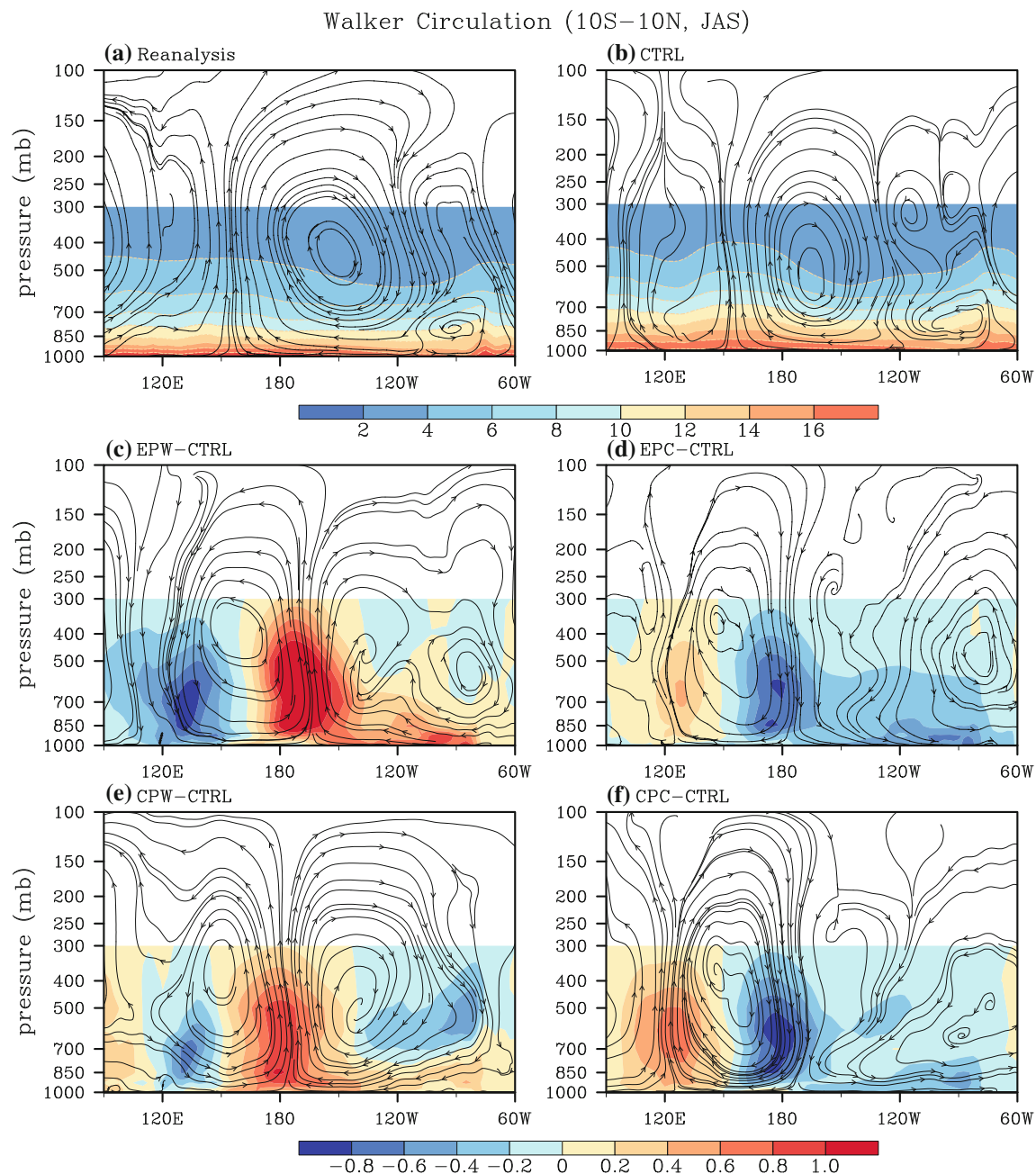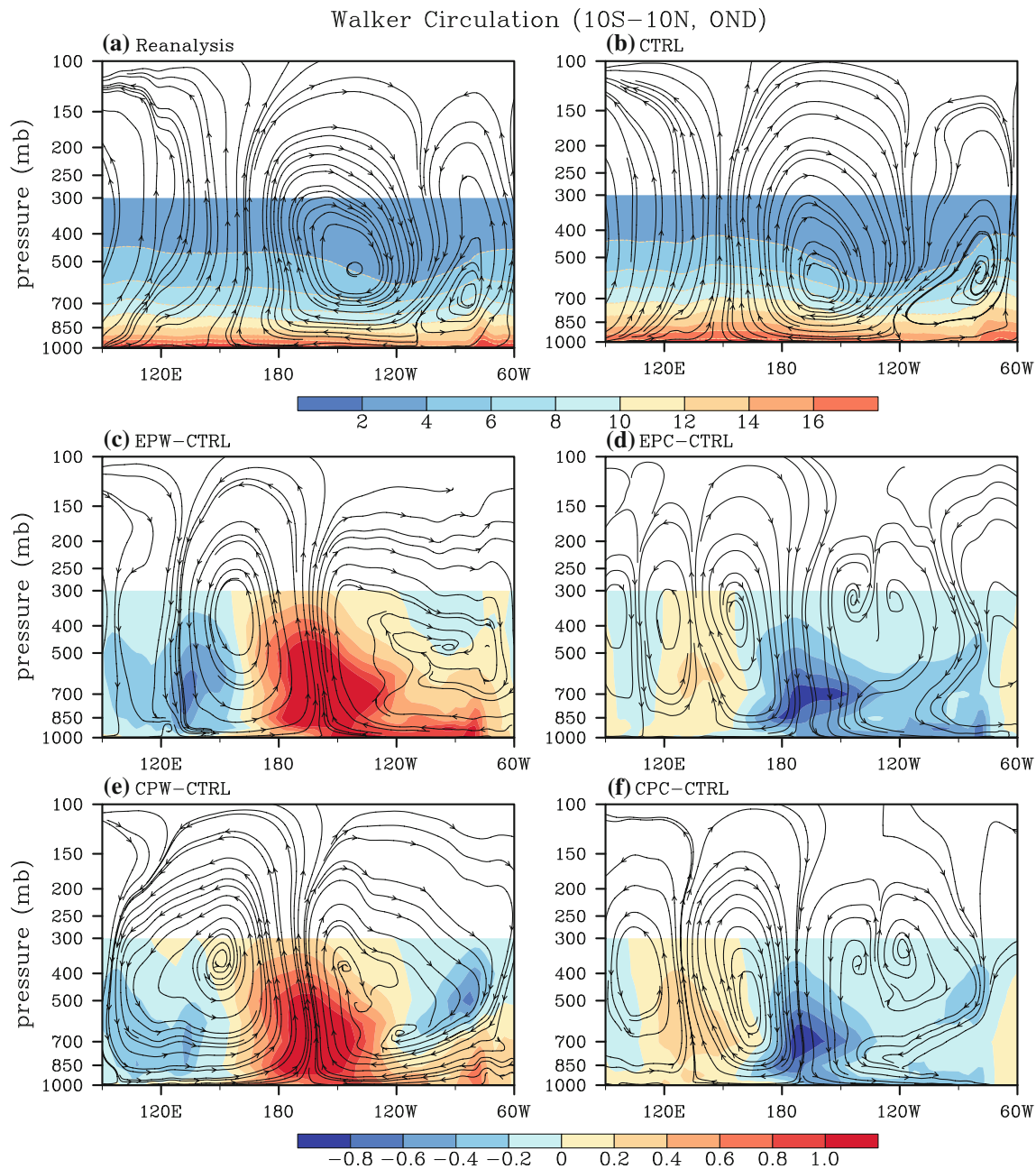
Fig. 10 The variations of the Walker circulation and specific humidity (*shading*; g/kg) during JAS. The Walker circulation is calculated by averaging divergent wind and vertical velocity between 10°S and 10°N. Shown are the climatological means from **a** the NCEP–NCAR reanalysis and **b** the CTRL ensemble run. The differences between the EPW, EPC, CPW, and CPC runs and the CTRL run are shown in **c**, **d**, **e**, and **f**, respectively

prevailed by the low-level easterly wind anomalies, which contribute to negative vorticity and suppression of the TC formation there, consistent with the observed reduction of the TC genesis in the SW sub-region of the WNP. However, both the narrow ascending and wide descending branches shift eastward and form a double-cell pattern during OND.

The CPC-induced Walker circulations are approximately similar to those in EPC events, except that the

anomalously dry descent in the east occupies a smaller domain and is much stronger (Figs. 10f, 11f). Therefore, a CPC event tends to create the environment more hostile to the TC development in the SE sub-region of the WNP (Fig. S1). Furthermore, the wet ascent over the western tropical Pacific retreats to the east of 120°E during OND, on account of the fact that the ascending motion is shifted northward off the tropics to the SCS, corresponding to

Fig. 11 The variations of the Walker circulation and specific humidity (*shading*; g/kg) during OND. The Walker circulation is calculated by averaging divergent wind and vertical velocity between 10°S and 10°N. Shown are the climatological means from **a** the NCEP–NCAR reanalysis and **b** the CTRL ensemble run. The differences between the EPW, EPC, CPW, and CPC runs and the CTRL run are shown in **c**, **d**, **e**, and **f**, respectively

enhanced TC activity observed in the SCS during OND (Fig. S1b).

6 Summary

The present paper extends the observed study of Wang et al. (2013) by using the AGCM of ECHAM5 to explore large-scale atmospheric response to various ENSO events

associated with TC activity in the WNP. Because of the short data period for the limited numbers of CPW/CPC events and the uncertainties of the observed TC data, it is necessary and important to use model experiments to confirm the observed results. Here we show that the model runs of various ENSO events are basically consistent with and confirm the observed results in Wang et al. (2013). For EPW, the Walker circulation depicts a circulation pattern with anomalously wet ascending flow in the eastern/central

Pacific and anomalously dry descending over the western Pacific, which manifests a reduced convection in the SW sub-region of the WNP and an enhanced convection in the SE sub-region. Meanwhile, associated with the variation of the Walker circulation, low-level westerly wind anomalies are located over the equatorial western to central Pacific, related to a positive relative vorticity and weakened VWS in the SE sub-region as well as strengthened VWS in the SW. In addition, an area of the positive GPI anomalies is situated in the SE sub-region, and the negative GPI anomalies are found in other sub-regions during JAS and OND. These factors consistently contribute to the increase in cyclogenesis in the SE sub-region, but the suppression in the west portion. Correspondingly, there are significantly more TCs formed in the SE sub-region but less in the NW sub-region during JAS, and less in the SW and NW sub-regions during OND. Furthermore, the EPW-induced TC steering flow shows that the East Asian trough is deepened, followed by the remarkable westerly anomalies over the areas close to the coast of East Asian. This TC steering flow pattern decreases the likelihood for TCs to move northwestward or westward, consistent with the negative anomalies of TC track density observed in the NW sub-region.

For EPC, the Walker circulation is almost opposite to that of EPW during JAS. Thus, the tropical region in the WNP is covered by low-level the easterly wind anomalies and negative relative vorticity anomalies, consistent with the decrease of TC activity observed in the SW sub-region during JAS. Moreover, the simulated GPI anomalies are approximately a mirror image of EPW event over the WNP during JAS and OND, consistent with the observed increase of the TC formation in the NW and NE sub-regions during JAS, and the increase in the NW sub-region during OND. Consequently, the positive anomalies of TC track density are observed in the north of the WNP (Wang et al. 2013).

For CPW, the anomalous Walker circulation shifts westward in comparison with that of EPW because of the westward shift of the maximum SST anomaly forcing. During JAS, the distributions of relative vorticity, GPI, and VWS anomalies are favorable for TCs to form in the band orienting from the SE sub-region of the WNP to the southeast of China. Additionally, there is an anomalous anticyclone of the TC steering flow over the sea east of Japan and the westerly flow anomalies in the tropics, leading more northwestward but less westward TC tracks. Compared to JAS, the TC-favored area shifts southeastward and is confined to the SE sub-region where the TC development is promoted during OND. Meanwhile, the downdraft of the west branch of the Walker circulation shifts northward to the SCS during OND, inhibiting the TC formation there, consistent with the significant decrease of the TC number in the SCS during OND (Wang et al. 2013).

For CPC, the descending motion in the central/eastern Pacific is much stronger and more concentrated compared to the counterpart of EPC. Moreover, the stronger positive VWS anomalies and negative vorticity and GPI anomalies are found in the SE sub-region. Therefore, it is more effective in suppressing cyclogenesis in the SE sub-region during JAS and OND of CPC years. Meanwhile, the ascending branch over the western Pacific shifts to the SCS during OND, enhancing the TC formation there. The anomalous cyclonic TC steering flows are located over eastern China, and the easterly TC steering anomalies dominate the tropical region during JAS, enhancing TC activity in the east coast of China.

In summary, the model simulated low-level relative vorticity, wind, VWS, GPI, TC steering flow and Walker circulation show a high degree of consistency with the features of TC activity observed in the WNP in association with various ENSO events. However, there are also some regions in which not all changes of environmental parameters are consistent with the observations. Obviously, there is a need for a further investigation of the influences of various ENSO events on TC activity in the WNP. Such work may involve exploring the reproducibility of the results in other atmospheric models and analyzing the two types of ENSO events' influence based on coupled ocean-atmosphere-land models.

Appendix 1: Location of TC formation in observations

The composited TC number anomalies with the two types of ENSO events during the peak season of JAS and late season of OND over the different sub-regions are presented in Fig. S1. Dot (cross) filled bars indicate statistically significant above (below) climatology at the 90 % confidence level. During JAS, EPW corresponds to a significant increase (decrease) of TC genesis number in the SE (NW) sub-region. The TC genesis number in EPC year is reduced in the SW sub-region, whereas it is enhanced in the NW and NE sub-regions. CPW shows no statistically distinct difference of the TC genesis from climatology in all sub-regions, while CPC suppresses the formation in the SE sub-region. For the late season of OND, there is a significant decrease of the TC genesis number in the SW and NW sub-regions during EPW years, but an increase in the SE sub-

region during CPW years. ENSO influence on TCs formed in the SCS is pronounced only during the late season of OND. CPW (CPC) is associated with a decreased (increased) TC formation in the SCS during OND.

Appendix 2: TC track density and steering flow in observations

We calculate the TC track density in the WNP by counting the number of TCs forming within and passing through each $5°'5°$ grid box for a given season. The TC steering flow is calculated as the vertically-integrated wind from 850 to 300 hPa, normalized by (850–300-hPa). Figures S2 and S3 show the composites of TC track density and steering flow anomalies for EPW, EPC, CPW and CPC during JAS and OND, respectively. During JAS, associated with the positive and negative anomalies of TC track density in the SE and NW sub-regions for EPW events are the easterly and westerly steering flow anomalies, respectively (Fig. S2a). For EPC events, the positive anomalies of TC track density are found in the northern portion of the WNP (Fig. S2b), due to the EPC-induced increase of TC genesis there (Fig. S1a). For CPW events, an anomalous anticyclonic steering flow is located over the sea east of Japan, which favors TCs to move north-westward. Meanwhile, the westerly steering flow anomalies occupy the tropics, suppressing the westward movement (Fig. S2c). For CPC events, an anomalous cyclonic steering flow occupies the sea east of China, and easterly anomalies prevail in the tropics. Associated with these TC steering flow patterns, there is a zonal dipole of TC track density anomalies with positive values in the east coast of China and negative values in the eastern part of the WNP (Fig. S2d).

During OND, an anomalous anticyclonic steering flow is found over the Philippines in EPW events, which suppresses TC activity there (Fig. S3a). An EPC year shows almost a mirror image of the EPW distribution (Fig. S3b). For CPW events, the westerly anomalies of the TC steering flow prevail in the tropical WNP, corresponding to a decrease of TC track density over Indo-China, the SCS and Philippines (Fig. S3c). For CPC events, due to the increased number of TCs formed in the SCS, the positive anomalies of TC track density are located over the south-east coast of China. The negative anomalies of TC track density are in the eastern part of the WNP due to the decrease of TCs formed there during CPC years (Fig. S3d).

References

Ashok K, Yamagata T (2009) Climate change: the El Niño with a difference. Nature 461:481–484

Ashok K, Behera SK, Rao SA, Weng H, Yamagata T (2007) El Niño Modoki and its possible teleconnection. J Geophys Res 112:C11007. doi:10.1029/2006JC003798

Cai W, Cowan T (2009) La Niña Modoki impacts Australia autumn rainfall variability. Geophys Res Lett 36:L12805. doi:10.1029/2009GL037885

Camargo SJ, Sobel AH (2005) Western North Pacific tropical cyclone intensity and ENSO. J Clim 18:2996–3006

Camargo SJ, Sobel AH, Anthony AG, Barnston G, Emanuel KA (2007) Tropical cyclone genesis potential index in climate models. Tellus 59A:428–443

Chan JCL (2000) Tropical cyclone activity over the western North Pacific associated with El Niño and La Niña events. J Clim 13:2960–2972

Chen G (2011) How does shifting Pacific Ocean warming modulate on tropical cyclone frequency over the South China Sea? J Clim 24:4695–4700

Chen G, Tam C-Y (2010) Different impacts of two kinds of Pacific Ocean warming on tropical cyclone frequency over the western North Pacific. Geophys Res Lett 37:L01803. doi:10.1029/2009GL041708

Dong K, Neumann CJ (1986) The relationship between tropical cyclone motion and the environmental geostrophic flows. Mon Weather Rev 114:115–122

Emanuel KA, Nolan DS (2004) Tropical cyclone activity and global climate. In: Proceedings of 26th conference on hurricanes and tropical meteorology. American Meteorological Society, Miami, FL, pp 240–241

Gill AE (1980) Some simple solutions for heat-induced tropical circulation. Q J R Meteorol Soc 106:447–462

Gray WM (1979) Hurricanes: their formation, structure and likely role in the tropical circulation. In: DB Shaw (ed) Meteorology over the tropical oceans. Royal Meteorological Society, James Glaisher House, Bracknell, pp 155–218

Julian PR, Chervin RM (1978) A study of the Southern Oscillation and the Walker Circulation. Mon Weather Rev 106:1433–1451

Kalnay E et al (1996) The NCEP/NCAR 40-year reanalysis project. Bull Am Meteorol Soc 77:437–471

Kao HY, Yu JY (2009) Contrasting eastern Pacific and central Pacific types of 468 ENSO. J Clim 22:615–631

Kim H-M, Webster PJ, Curry JA (2009) Impact of shifting patterns of Pacific Ocean warming on north Atlantic tropical cyclones. Science 325:77–80

Kim H-M, Webster PJ, Curry JA (2011) Modulation of North Pacific tropical cyclone activity by three phases of ENSO. J Clim 24:1839–1849

Kug J-S, Jin F-F, An S-I (2009) Two-types of El Niño events: cold tongue El Niño and WARM POOL El Niño. J Clim 22:1499–1515

Larkin NK, Harrison DE (2005) Global seasonal temperature and precipitation anomalies during El Niño autumn and winter. Geophys Res Lett 32:L16705. doi:10.1029/2005GL0

Larson S, Lee S-K, Wang C, Chung E-S, Enfield D (2012) Impacts of non-canonical El Niño patterns on Atlantic hurricane activity. Geophys Res Lett 39:L14706. doi:10.1029/2012GL052595

Lee S-K, Wang C, Enfield DB (2010) On the impact of central Pacific warming events on Atlantic tropical storm activity. Geophys Res Lett 37:L17702. doi:10.1029/2010GL044459

Rayner NA, Parker DE, Horton EB, Folland CK, Alexander LV, Rowell DP, Kent EC, Kaplan A (2003) Global analyzes of SST, sea ice, and night marine air temperature since the late nineteenth century. J Geophys Res 108:4407. doi:10.1029/2002JD002670

Roeckner E, Baeuml G, Bonaventura L, Brokopf R, Esch M, Giorgetta M, Hagemann S, Kirchner I, Kornblueh L, Manzini E, Rhodin A, Schlese U, Schulzweida U, Tompkins A (2003) The

general circulation model ECHAM5. Part I: model description. Report 349, Max-Planck-Institut for Meteorology, Hamburg

Wang B, Chan JCL (2002) How strong ENSO events affect tropical storm activity over the western North Pacific. J Clim 15: 1643–1658

Wang C, Wang X (2013) Classifying El Niño Modoki I and II by different impacts on rainfall in the southern China and typhoon tracks. J Clim 26:1322–1338

Wang C, Weisberg RH, Virmani JL (1999) Western Pacific interannual variability associated with the El Niño-Southern Oscillation. J Geophys Res 104:5131–5149

Wang C, Li C, Mu M, Duan W (2013) Seasonal modulations of different impacts of two types of ENSO events on tropical cyclone activity in the western North Pacific. Clim Dyn 40:2887–2902

Wang C, Deser C, Yu J-Y, DiNezio P, Clement A (2014) El Niño-Southern Oscillation (ENSO): a review. In: Glymn P, Manzello D, Enochs I (eds) Coral Reefs of the Eastern Pacific. Springer Science Publisher (in press)

Weisberg RH, Wang C (1997) A western Pacific oscillator paradigm for the El Niño-Southern Oscillation. Geophys Res Lett 24:779–782

Weng H, Ashok K, Behera SK, Rao AS, Yamagata T (2007) Impacts of recent El Niño Modoki on dry/wet conditions in the Pacific rim during boreal summer. Clim Dyn 29:113–129

Weng H, Behera SK, Yamagata T (2009) Anomalous winter climate conditions in the Pacific rim during recent El Niño Modoki and El Niño events. Clim Dyn 32:663–674

Wu M, Chang W, Leung W (2004) Impacts of El Nino-Southern Oscillation events on tropical cyclone landfalling activity in the western North Pacific. J Clim 17:1419–1428

Yu J-Y, Kao H-Y (2007) Decadal changes of ENSO persistence barrier in SST and ocean heat content indices: 1958–2001. J Geophys Res 112:D13106. doi:10.1029/2006JD007654

Yu J-Y, Kim ST (2010) Three evolution patterns of Central-Pacific El Niño. Geophys Res Lett 37:L08706. doi:10.1029/2010GL 042810

Zhang W, Graf H, Leung Y, Herzog M (2012) Different El Niño types and tropical cyclone landfall in East Asia. J Clim 25:6510–6523

Zhao HK, Wu LG, Zhou WC (2010) Assessing the infuence of the ENSO on tropical cyclone prevailing tracks in the western North Pacific. Adv Atmos Sc 27:1361–1371